

# TWO-DIMENSIONAL SIMULATIONS OF CONTAMINANT CURRENTS IN STRATIFIED RESERVOIR

By Se-Woong Chung<sup>1</sup> and Ruochuan Gu,<sup>2</sup> Associate Member, ASCE

**ABSTRACT:** An unsteady two-dimensional (2D) reservoir hydrodynamics and transport model is employed to simulate contaminated density currents in the Shasta Reservoir after a chemical spill into the Sacramento River, Calif. Three flow regimes (plunging flow, underflow, and interflow) and their occurrence are captured by the laterally averaged model. Transport and mixing processes in the temperature-stratified reservoir are analyzed through simulations of flow velocities, water temperature, and contaminant concentration. Flow behavior of the contaminant plume is described by plunge distance, separation depth, intruding thickness, and the spatial and temporal dilution of chemicals. Simulation results are compared with field data for water temperature and contaminant concentration collected in the reservoir during the emergency response to the spill. Relatively good agreement between field measurements and predicted reservoir stratification and chemical dilution is obtained. It is shown that the aeration system installed in the reservoir contributed to the downstream reduction of chemical concentration to a nondetectable level shortly after the spill. The 2D simulations and analyses improve understanding and predictions of the movement of a conservative contaminant plume in a stratified reservoir. The results can assist in contamination control and remediation after a toxic chemical spill, guide field sampling during the spill, and provide information useful for water quality management.

## INTRODUCTION

A reservoir's water quality conditions after a toxic chemical spill into an upstream river are influenced by physical processes as well as biochemical reactions. After the chemical enters the river, transport and kinetic processes cause the material to move, disperse, and degrade, resulting in a reduction of contaminant concentration when arriving at the reservoir. The ultimate fate depends not only on the nature of the spilled chemicals but also on the characteristics of the river flow carrying the spill and the ambient and boundary conditions of the reservoir. The density differences between incoming river water and ambient reservoir water and between reservoir layers may alter behavior of the spilled chemical plume. After entering the reservoir, river flow contaminated by spilled chemicals may plunge (Akiyama and Stefan 1984; Johnson et al. 1989; Fang and Stefan 1991) and form an underflow, depending on the buoyant force (Hebbert et al. 1979; Alavian et al. 1992). In a density-stratified reservoir, an interflow occurs after the underflow separates from the riverbed and intrudes into a layer where the flow is neutrally buoyant (Fisher et al. 1979; Imberger 1982; Imberger and Hamblin 1982; Ford and Johnson 1983). Different reservoir flow patterns result in different processes of transport and dilution of toxic chemicals (Gu et al. 1996). A full understanding and accurate predictions of spill behavior in various flow regimes is important to contamination control and remediation management.

Alavian and Ostrowski (1992) investigated the use of density current to modify the thermal structure of Tennessee Valley Authority reservoirs. Van Gils (1988) conducted toxic chemical spill modeling as a management tool for the Rhine River. A one-dimensional (1D) simulation model for chemical spills and pesticide release to large rivers was developed by Schnoor et al. (1992) and Mossman et al. (1988). The method by Van Gils (1988) and the 1D model by Schnoor et al. (1992) are primarily limited to transport in long and shallow rivers.

<sup>1</sup>Res. Asst., Dept. of Civ. and Constr. Engrg., Iowa State Univ., Ames, IA 50011.

<sup>2</sup>Asst. Prof., Dept. of Civ. and Constr. Engrg., Iowa State Univ., Ames, IA.

Note. Discussion open until December 1, 1998. To extend the closing date one month, a written request must be filed with the ASCE Manager of Journals. The manuscript for this paper was submitted for review and possible publication on March 17, 1997. This paper is part of the *Journal of Hydraulic Engineering*, Vol. 124, No. 7, July, 1998. ©ASCE, ISSN 0733-9429/98/0007-0704-0711/\$8.00 + \$.50 per page. Paper No. 15465.

Modeling efforts were made during the 1991 Sacramento River chemical spill, which entered the Shasta Reservoir, Calif. An integral simulation model was developed by Gu et al. (1996). The simplicity of the model makes it suitable as a screening tool for assessing contamination levels at different locations as a first approximation during a spill emergency.

The various flow regimes of a contaminated density current in a stratified reservoir are multidimensional phenomena, which, particularly interflow, have not been simulated and analyzed using a two-dimensional (2D) or three-dimensional (3D) numerical model. A spill to a river or reservoir usually is an impulse loading process. Plunging, separation, and intrusion of the spilled chemical plume are transient processes. Therefore, a 2D unsteady model is required for better understanding and more accurate predictions of the contaminant plume's movement and for simulating interflow. The model should be capable of predicting the occurrence of the various flow regimes and describing their behavior in detail. Although model complexity, time constraints, and data availability may limit the use of a 2D or 3D model during a spill, it is necessary and feasible in a pre- or postspill study with a sufficient amount of time and data.

In this study, an unsteady 2D reservoir hydrodynamics and transport model is used to describe contaminated density currents and to simulate mixing and transport of a spilled conservative chemical plume in the stratified Shasta Reservoir. The reservoir is simulated as a whole flow domain by means of using the laterally averaged model. The occurrence of three flow regimes (plunging flow, underflow, and interflow) is identified and their behavior is captured by analyzing the model results. The simulated velocity fields and concentration distributions over space and time are used to determine plunging distance, separation depth of underflow, intruding thickness of interflow, dilution of contaminants, travel time, and propagation speed of the contaminant plume. The simulations provide insight into the processes controlling the spread of the spill and the transport of the plume. The 2D model results are compared with field measurements of water temperature and contaminant concentration in the Shasta Reservoir and with previous computations using the 1D integral method.

## MODEL DESCRIPTION

The generalized longitudinal-vertical hydrodynamics and transport (GLVHT) model (Buchak and Edinger 1984; Environmental 1986) was used in this study. GLVHT was devel-

oped from the laterally averaged reservoir model (LARM) and has been used to derive a water quality model, CE-QUAL-W2, that directly couples hydrodynamics and water quality algorithms (Cole and Buchak 1994). The model has been tested against field data and applied to stratification and water quality problems such as dissolved oxygen, nutrients, and eutrophication in lakes and reservoirs (Cole 1982; Edinger et al. 1983; Martin 1987; Mckee et al. 1992; Barnese et al. 1993). The model has not been used, however, to simulate and analyze a contaminant density current (plunge, underflow, and interflow) in a reservoir after a chemical spill.

In the model, 2D advection-diffusion equations describing laterally averaged fluid motion and mass transport are solved by using the finite-difference method. The dependent variables are water surface elevation ( $n$ ), pressure ( $P$ ), density ( $\rho$ ), horizontal and vertical velocities ( $U$  and  $W$ ), and constituent concentrations ( $C$ ). The independent variables are longitudinal distance ( $x$ ), flow depth ( $z$ ), and time ( $t$ ). The governing equations in a 2D Cartesian coordinate system are

For horizontal momentum

$$\frac{\partial(UB)}{\partial t} + \frac{\partial(UUB)}{\partial x} + \frac{\partial(WUB)}{\partial z} = -\frac{1}{\rho} \frac{\partial(BP)}{\partial x} + \frac{\partial}{\partial x} \left( BA_x \frac{\partial U}{\partial x} \right) + \frac{\partial(B\tau_x)}{\partial z}$$

For constituent transport

$$\frac{\partial(BC)}{\partial t} + \frac{\partial(UBC)}{\partial x} + \frac{\partial(WBC)}{\partial z} - \frac{\partial}{\partial x} \left( BD_x \frac{\partial C}{\partial x} \right) - \frac{\partial}{\partial z} \left( BD_z \frac{\partial C}{\partial z} \right) = q_c B + S_c B$$

For free water surface elevation

$$\frac{\partial(B_n \cdot n)}{\partial t} = \frac{\partial}{\partial x} \left( \int_n^h UB dz \right) - \int_n^h qB dz$$

For hydrostatic pressure

$$\frac{\partial P}{\partial z} = \rho g$$

For continuity

$$\frac{\partial(UB)}{\partial x} + \frac{\partial(WB)}{\partial z} = qB$$

For density

$$\rho = f(T_w, C_{TDS}, C_{SS})$$

The vertical turbulent dispersion coefficient ( $D_z$ ) is determined by using the concept of eddy viscosity with the mixing length model.  $D_z$  is calculated from velocity gradient, depth, water density distribution or reservoir stratification, bottom shear, and surface wind shear (Buchak and Edinger 1984; Cole and Buchak 1994). A stable stratification hampers the vertical movement of water and constituents. The effect of stratification on turbulent transport is taken into account by correction to  $D_z$  under nonstratified conditions with a local Richardson number defined by velocity and density gradients (Orlob 1983; Cole and Buchak 1994). A default value (1 m<sup>2</sup>/s) for the longitudinal dispersion coefficients ( $A_x$  for momentum and  $D_x$  for mass) is used in this study. The default value is based on model testing against field data for numerous reservoirs under a wide variety of conditions (Cole and Buchak 1994).

The laterally averaged model is appropriate for water bodies where lateral variations in velocity and temperature are insignificant. It is applicable to a reservoir with a side expansion angle less than 7°, where a plunge flow can be assumed as a

2D process (Johnson et al. 1987; Alavian et al. 1992). In a stratified flow situation, the flow may still remain attached to the side boundaries with an expansion angle larger than 7° because of the horizontal spreading forces.

Another limitation of the model is that the vertical momentum equation is simplified by assuming hydrostatic pressure (Cole and Buchak 1994). Vertical acceleration of water in a reservoir is driven by gravity (on a steep slope) as well as buoyancy of the flow. However, if the bottom slope is less than 5%, the vertical momentum becomes insignificant and the hydrostatic pressure assumption may be valid (Chow 1959; Chaudhry 1993), provided that other processes, e.g., wind mixing and instability of stratification, are weak. In the application to the Shasta reservoir (slope = 0.3%), the hydrostatic pressure assumption is valid for the regions of underflow and interflow (horizontal intruding), where vertical acceleration has subsided. Little is known about dynamic pressure near the plunge point where the flow is vertical. Farrell and Stefan (1989) performed mathematical modeling of plunging reservoir flow without the hydrostatic assumption and derived a plunge depth and mixing coefficient from simulated velocity and temperature fields. Unfortunately, the feature of pressure in the plunge region was not explored.

## APPLICATION TO SHASTA RESERVOIR

### Study Area

Shasta Reservoir has a  $1.9 \times 10^9$  m<sup>3</sup> capacity and regulates the Sacramento River (Fig. 1). The average longitudinal river bed slope and reservoir side expansion angle are 0.3% and 1°, respectively. The reservoir is approximately 109 m deep at the dam wall and extends along the Sacramento River Valley (Table 1). The reservoir is temperature stratified during the summer. Vertical stratification was relatively stable during the July 1991 spill. The observed temperatures in the Shasta Reservoir showed that vertical and longitudinal variations are significant, but lateral variations are generally small in the upper reach from the head of the reservoir to its confluence with the Squaw River arm (Chung 1996). Water temperatures in the reservoir were in the range of 19–27.5°C in the epilimnion and 7–16°C in the hypolimnion. The river flow entering the reservoir averaged 7.5 m<sup>3</sup>/s with a temperature of 18–24°C during the spill. The corresponding flow parameters, i.e., Reynolds number, densimetric Froude number, and flow velocity, were estimated as 107,000, 0.7–1.03, and 0.107 m/s, respectively.

### Spill

On July 15, 1991, between 49,000 and 72,000 L of VAPAM liquid formulation were estimated to have spilled into the Sacramento River, Calif. (Fig. 1), about 48 km upstream from the Shasta Reservoir (Rosario et al. 1994). VAPAM, sodium methyl dithiocarbamate (Na-MDTC), is a fumigant with a fungicidal, nematicidal, and herbicidal action (Worthing 1987). The parent compound Na-MDTC decomposes quickly (in 5–6 h) into more stable products, primarily the far more toxic chemical methyl isothiocyanate (MITC) in water with a specific weight of 1.0691 (Lide 1992). Other by-products included methylamine or hydrogen sulfide. The spill prompted emergency responses from 35 public agencies because MITC is toxic to humans and aquatic life. Water sampling activities were conducted by the California Regional Water Quality Control Board to keep track of the spill in the Sacramento River after it entered the Shasta Reservoir (Fig. 2). The field measurements also served to determine the contamination level of the water body and the speed at which the spilled chemical plume was moving in the river and reservoir toward the Shasta Dam.

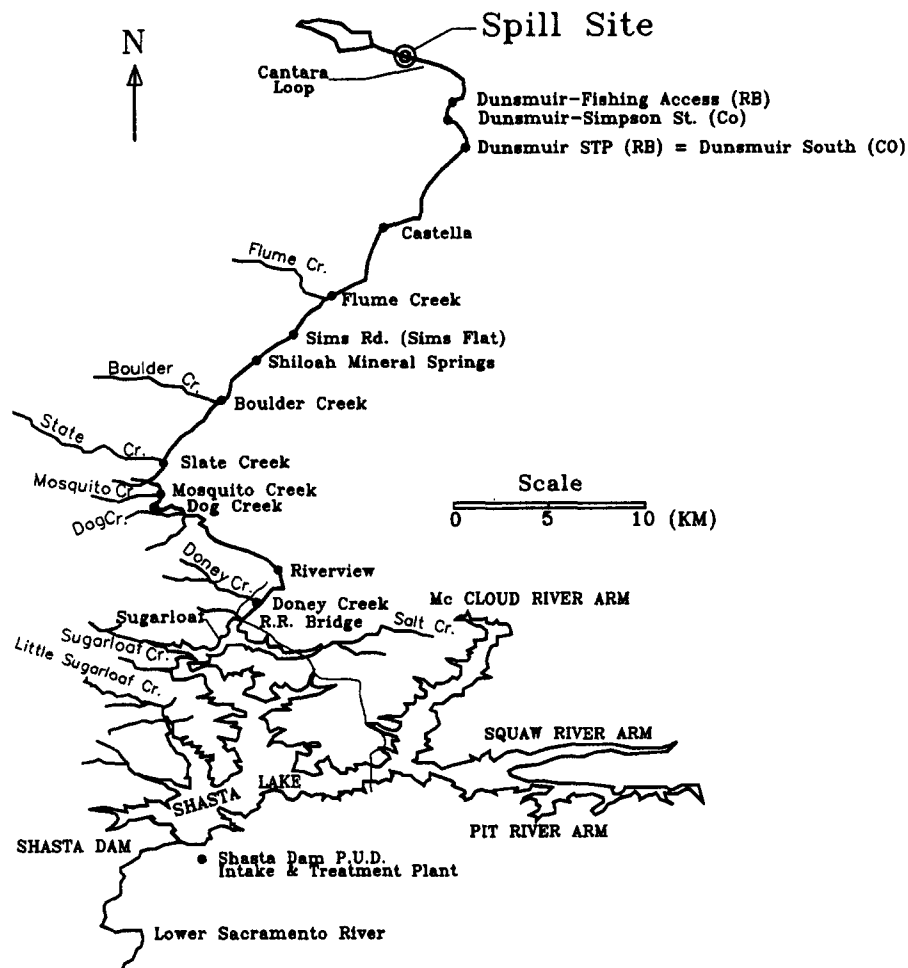


FIG. 1. Map of Sacramento River, Shasta Reservoir, and Spill Site

TABLE 1. Geometry of Shasta Reservoir, Model Segments, and Field Sampling Stations

Segment number (1)	Distance from Shasta Dam (km) (2)	Distance increment (km) (3)	Reservoir width (km) (4)	Reservoir depth (m) (5)	Sampling station number (6)
2	20.2	0.2	0.07	1	—
3	20.0	0.2	0.07	2	—
4	19.8	0.2	0.07	4	1
5	19.6	0.2	0.07	5	—
6	19.4	0.2	0.07	6	—
7	19.2	0.2	0.07	7	—
8	18.9	0.3	0.08	8	2, 3
9	18.6	0.3	0.09	10	4
10	18.2	0.4	0.11	13	5
11	17.7	0.5	0.12	16	6, 7, 8
12	17.2	0.5	0.15	19	9
13	16.7	0.5	0.17	22	10, 11
14	16.2	0.5	0.18	24	12
15	15.7	0.5	0.20	28	13
16	15.2	0.5	0.25	32	14
17	14.2	1.0	0.30	36	15, 16
18	13.2	1.0	0.35	42	17, 18
19–32	12.2–0.0	1.0	0.40–1.60	48–109	—

### Computational Domain and Simulation Period

Insignificant lateral variation, small expansion angle, mild bottom slope, and stable stratification make it appropriate to apply the laterally averaged 2D model to the upper reach of the Shasta Reservoir, but not to the lower reach, where lateral variations can be significant due to the major tributaries or arms and a 3D model is needed. Only one major arm (the tributary between stations 7 and 8) is identified in the 10-km reach. Because the upper reach is long enough, possible un-

derflow, interflow, and dilution of the contaminant plume might occur within this reach (Fig. 2). Very low to undetectable chemical concentrations at Stations 17 and 18 are indicated by field measurements carried out during the spill. Simulations and comparison with data should be limited to the upper reach, where field measurements are available and primary mixing and transport take place. However, it is very difficult to specify the boundary conditions at an arbitrarily determined point that separates the upper reach from the lower one. Therefore, a computational domain from Doney Creek at the head of the reservoir to the Shasta Dam (Fig. 1) was used in the model application. With the whole reservoir domain, the well-defined boundary conditions at the dam can be utilized in the model.

A finite-difference grid system was generated, consisting of 32 segments with lengths of 200–1,000 m in the longitudinal direction and 52 vertical layers with thickness of 0.5–4 m (Table 1). The nonuniform grid system has finer grids in the plunging region and coarser grids in other regions. Reservoir widths are obtained from a map. The inflow width and depth at Doney Creek was 70 and 1.0 m, respectively. July 16–24, 1991 was chosen as the simulation period because the field measurements of MITC dropped to a nondetectable level after July 24, 1991. Variable time steps were used in the simulations, which are a fraction of the maximum time step calculated from the numerical stability criterion with an autosteping algorithm.

### Boundary and Initial Conditions

Unsteady MITC concentrations were specified at the upper end (Doney Creek) of the computational domain as the up-

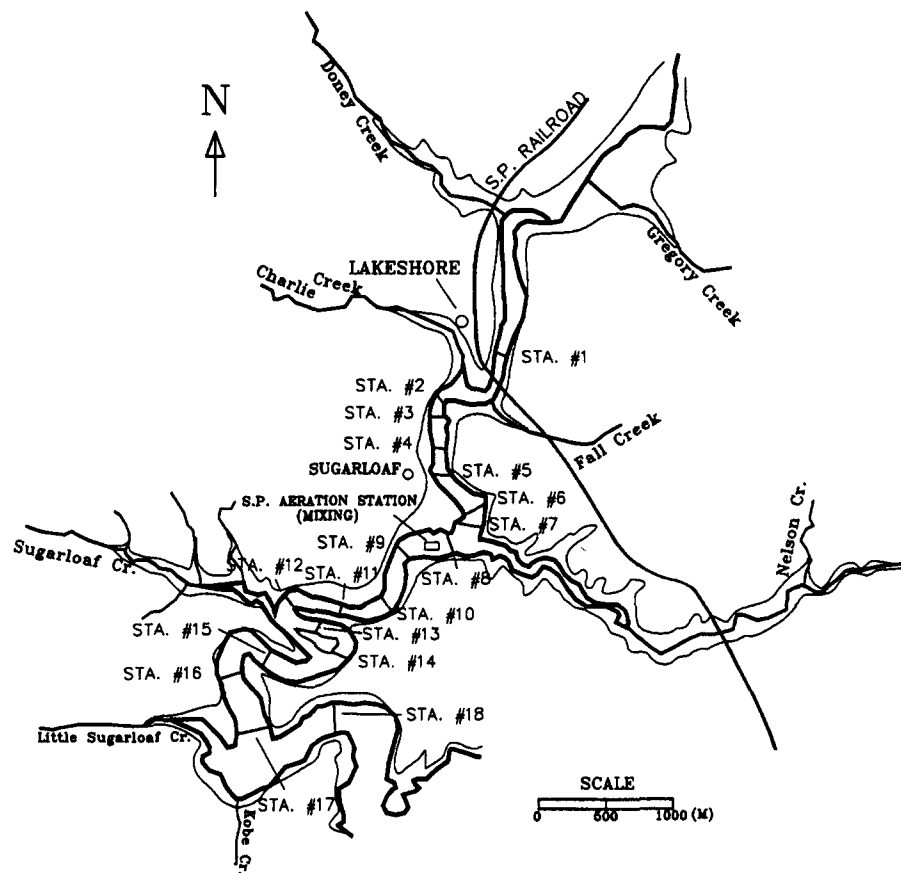


FIG. 2. Sampling Stations in Shasta Reservoir

stream boundary condition. Chemical concentration sampling was conducted on an hourly basis from midnight of July 16, when the plume arrived at Doney Creek, to 10:10 a.m. the next day, only three measurements were taken from then until noon July 19. The peak concentration ( $C_0$ ) passed Doney Creek at 5:00 a.m. on July 17. Most of the chemical plume had entered the reservoir by 10:00 a.m. on July 17. The measured inflow MITC concentration at the reservoir head varied with time, from 2 mg/L at midnight on July 16 to 35 mg/L (peak) at 5:00 a.m. and 5 mg/L at 10:00 a.m. on July 17, and dropped to a nondetectable level ( $<0.001$  mg/L) at noon on July 19. The flow boundary condition at the upstream end of the reservoir (Doney Creek) was a constant discharge of  $7.5$  m<sup>3</sup>/s during the simulation period. Outflow at the downstream boundary of the computational domain is assumed to be equal to the inflow discharge because variations in reservoir storage were insignificant during the simulation period. The initial MITC concentration in the reservoir was assumed as zero. The initial temperatures were calculated from field measurements using a linear interpolation (Chung 1996).

Nighttime convective mixing is an important physical process affecting epilimnetic depth and thermocline. Daily maximum and minimum temperatures rather than daily average air temperatures were used for the boundary condition at the water surface and were interpolated for each time step. Based on model calibration and values for mountain terrains, a wind sheltering coefficient of 0.85, a surface solar radiation absorption coefficient of 0.45, and an extinction coefficient of 0.40 were adopted.

## RESULTS OF MODEL SIMULATIONS

Simulations were conducted for water temperature, density, flow velocity, and MITC concentration throughout the reservoir over time. MITC was simulated as a conservative tracer.

It is assumed that the dilution of MITC in different reservoir flow regimes was caused mainly by transport processes, i.e., diffusion and advection. The tracer was used to evaluate the effects of mixing on material distributions and to predict flow behavior of the contaminant plume. The locations of plunging point and separation point, intruding depth and thickness, and chemical dilution were determined from the simulated velocities and MITC concentrations.

MITC is one of the more stable products of the spilled NAMDTC after traveled, dispersed, and reacted in the 48-km Sacramento River from the spill site for about two days to the reservoir (Rosario et al. 1994). Although it is known that MITC is a volatile and reactive compound when exposed to elevated temperature, oxygen level, and sunlight, its kinetic decay (volatilization, photolysis, and hydrolysis) in surface waters has not been well characterized (Rosario et al. 1994). Draper and Wakeham (1993) conducted laboratory experiments on the stability of MITC and found that 73% remained after 19 days at 25°C, a first-order (bottle) rate of  $0.015$  day<sup>-1</sup>. Direct photolysis at 1-m depth was estimated as about 5% of that at the water surface by Zepp and Cline (1977). After the spill plunged into the deep reservoir where volatilization may be negligible, forming underflow and interflow (1–10 m below water surface), MITC should have become relatively stable and nonreactive because of low water temperature, oxygen level, and sunlight for hydrolysis and photolysis. Although a slow degradation of MITC may have continued after the spill entered the reservoir, this process was assumed insignificant so that MITC could be simulated as a conservative contaminant.

Longitudinal propagation and vertical spreading of the contaminant plume are illustrated by the simulated MITC concentrations presented in Figs. 3 and 4. Fig. 4 shows predicted MITC concentration profiles at various sections at 8:00 a.m. on July 17, 1991 in different flow regimes about 3 h after the

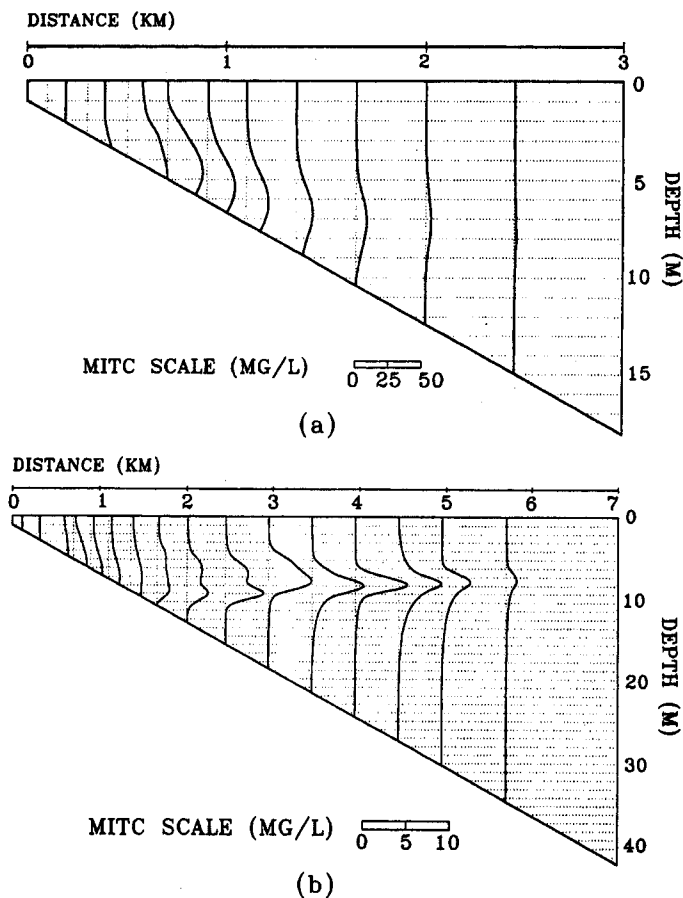


FIG. 3. Simulated MITC Concentrations (a) at Noon on 7/17/91; (b) at Noon on 7/18/91

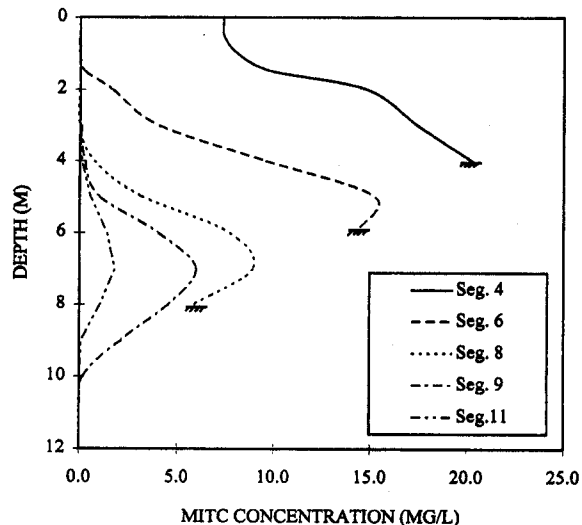


FIG. 4. Simulated Vertical Profiles of MITC Concentrations at Segments 4, 6, 8, 9, and 11 at 8:00 a.m. on 7/17/91

spill peak arrived at the reservoir head. Fig. 3(a) shows the situation at noon on July 17, about 7 h after the peak entered the head. During this first day, the plume is characterized by underflow penetration after plunging [Fig. 3(a)]. The behavior of the plume at noon on July 18 is described by interflow intruding after separation from the river bed [Fig. 3(b)]. The contaminated river water plunged between segments 4 and 6 at a distance of ~600–700 m downstream from the inflow boundary as the colder river water was arrested by buoyancy forces. The propagation of underflow along the reservoir bottom is seen in the region covered by segments 5, 6, 7 and 8.

During the underflow penetration, significant dilution of spilled chemicals occurred. The underflow continued until the diluted riverine water attained a density equal to the ambient water density at 5–10 m depth, where the underflow found its equilibrium layer. As shown in Fig. 4, the underflow separated from the reservoir bottom at the distance of 1,800 m downstream from the inflow point between segments 8 and 9 and at a depth of 8.5 m below the reservoir water surface. The results are consistent with the separation distance of 1,900 m predicted using a 1D integral model by Gu et al. (1996).

The mixing and transport of the plume are displayed by the simulated contours of MITC concentrations during the period of July 17–20 (Fig. 5). Plunging and underflow can be seen in Fig. 5(a). Separation and intrusion of the density plume on July 18 and 19 is seen in Figs. 5(b) and 5(c). On July 20, 1991, the contaminated density plume was isolated in the reservoir by the successive reintrusion of fresh river water, and the core of the plume was located 7 km downstream from the reservoir head [Fig. 5(d)]. The plume separated from the bottom, formed an interflow, and propagated horizontally at a depth of 7–8 m in the reservoir on July 17, 1991. The contour plots of MITC in the reservoir clearly show that dilution of the plume by mixing with ambient water occurred while it spread vertically and propagated in the longitudinal direction.

An interflow with uniform thickness of approximately 7 m is identified in the 2D simulation results. The thickness of an interflow is defined as the vertical distance between two points, where the concentration is 10% of the maximum concentration at the plume centerline. The intruding thickness

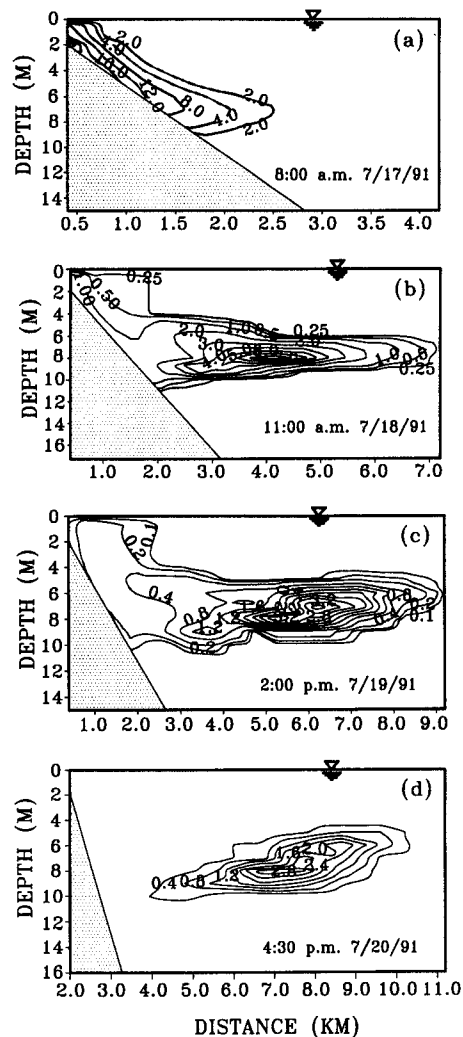


FIG. 5. Simulated MITC Concentration Contours

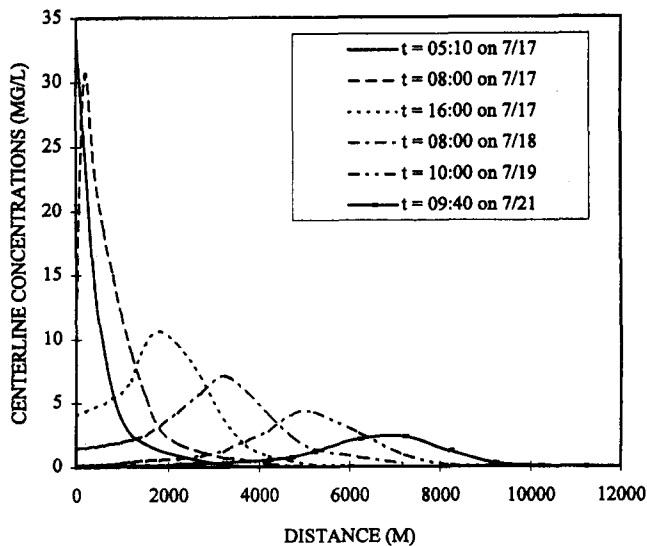


FIG. 6. Simulated Centerline MITC Concentrations Showing Longitudinal Propagation of Spilled Chemical Plume

changed very little with distance according to the 2D model simulations. The reason for this is that summer stratification may confine the vertical spread of interflow in a stratified reservoir. The integral model based on an empirical equation predicted a variable intruding thickness from 6.0 m at the separation point and 9.5 m at the dam face (Gu et al. 1996).

The predicted centerline concentrations in the Shasta Reservoir at various times are presented in Fig. 6. The maximum concentrations at each section are plotted against the longitudinal distance. The sharp pulse chemical loading at the inflow boundary spreads in along the flow direction due to transport and mixing processes. The peak concentration of the plume is considerably attenuated while it plunges and propagates. The simulation results demonstrated the capability of the 2D model in describing flow behavior and predicting the mixing processes and dilution patterns of a contaminant plume in different flow regimes in a stratified reservoir.

#### COMPARISON WITH FIELD DATA

Simulation results are compared with field measurements and observations of water temperatures and MITC concentrations in the Shasta Reservoir. Because hydrodynamic field data are not available, direct verification of the model hydrodynamic results is impossible. Because the transport of MITC is governed by these hydrodynamics, it would be unlikely that meaningful simulation results of the contaminant concentration be obtained by using inaccurate hydrodynamic transport information. Therefore, good comparisons of water temperatures and MITC concentrations can be used as indirect evidence of the model's predictive capability.

The vertical profiles of measured and simulated water temperatures in the Shasta Reservoir for selected sampling stations (2, 8, 13, and 17) during July 19–23 are compared in Fig. 7. The difference in the depth scale of Fig. 7 should be noted. Measured water temperatures at three transverse distances at each depth were averaged for comparison with simulated temperatures. Although the overall temperature dynamics and reservoir stratification were correctly simulated, there are some discrepancies between measured and simulated temperatures at Sampling Station 13 on July 22. Shasta Reservoir at Station 13, downstream of the confluence with one of its tributaries (Sugarloaf Creek), becomes wide and braided. Water samplings for temperature and chemical data were taken only in the right channel at the station. In addition the surface layer temperatures at all stations were overpredicted, whereas the

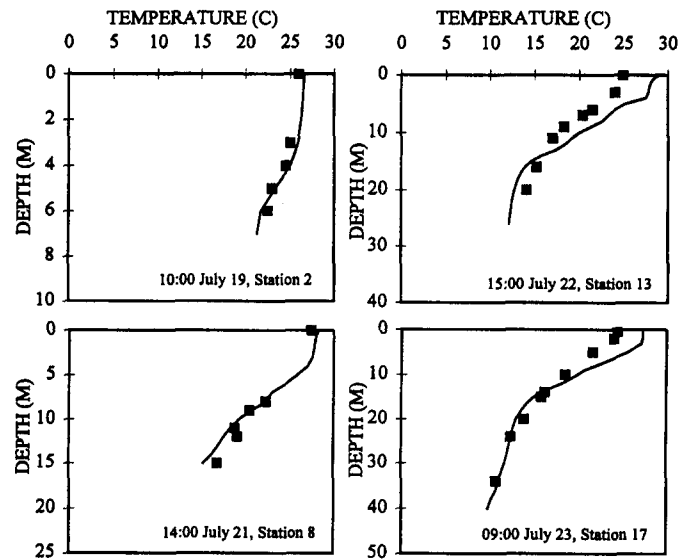


FIG. 7. Measured (Squares) and Simulated (Solid Lines) Reservoir Water Temperatures

simulated temperatures in the deep layers were slightly lower than those observed. The deviations between field measurements and model results for the surface layer may be attributed to the overestimation of absorbed solar radiation and the underestimation of heat losses from the water to the air.

Observed and simulated vertical profiles of MITC concentrations are presented in Fig. 8. It is shown that the chemical

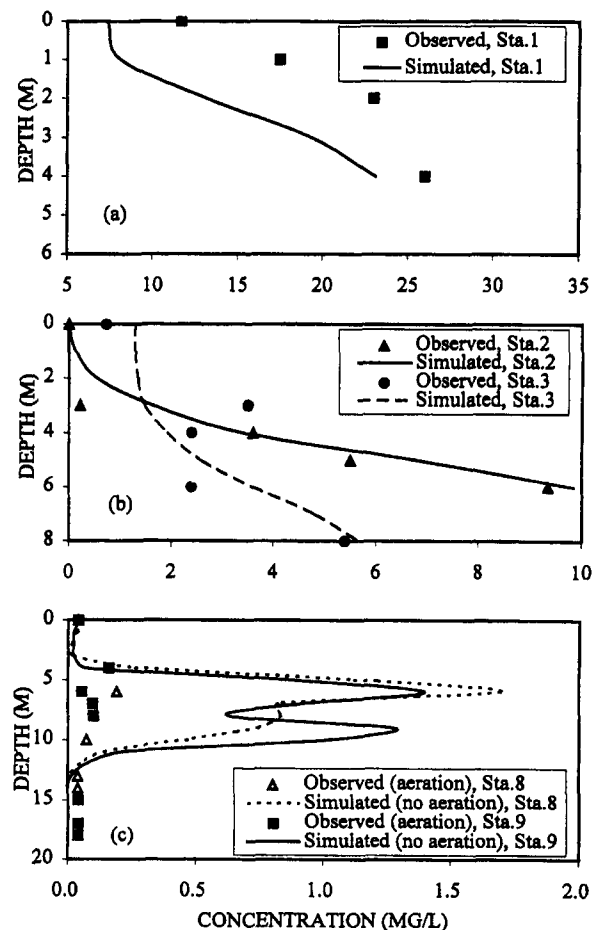


FIG. 8. Observed and Simulated MITC Concentration Profiles at (a) Sampling Station 1 at 8:30 on July 17; (b) Stations 2 and 3 at 16:50 on July 17 and 9:30 on July 18; (c) Station 8 at 16:20 on July 18 and Station 9 at 14:00 on July 19

plume plunged near the head of the reservoir and formed an underflow and an interflow in the layers of 6.0–9.0 m below the water surface. The development of underflow can be seen at Stations 1 and 2 on July 17, and Station 3 on July 18 [Figs. 8(a) and 8(b)]. The interflow propagation appeared at Stations 8 and 9 on July 18 and 19 [Fig. 8(c)]. The differences between measurements at Stations 8 and 9 and model results [Fig. 8(c)] are attributed to an aeration system installed just upstream after the chemical spill to artificially mix the contaminant plume with reservoir water. The simulations did not include the effect of artificial aeration on mixing or dilution. Some disagreement near the reservoir surface may be caused by the inaccurate prediction of epilimnetic mixing, which is affected by wind direction for which data are unavailable. The chemical was also observed at depths greater than 12 m after July 18 [Fig. 8(c)]. The MITC detected at the deep layers might result from the settling of a small amount of MITC because its density ( $1,069.1 \text{ kg/m}^3$ ) is slightly greater than that of water.

A split of the plume near the centerline of the plume at a depth of 7–8 m at Station 9 after July 19 was identified by the 2D model. As seen in Fig. 8(c), the MITC concentrations at the centerline of the interflow decreased considerably. This might be caused by the continuous intrusion of fresh water from upstream river into the contaminated plume interflow after the spill peak passed the reservoir head. The velocity differences between the center and boundaries of the interflow might be responsible for the split of the plume as an interflow. The higher velocity at the centerline of the interflow could have brought more fresh water to the plume and led to more dilution within the center layer of the interflow (Fig. 5).

Presented in Fig. 9 are observed and simulated MITC plume concentrations ( $C_m$ ) at different stations at times the plume passed. The results obtained by the 1D integral model (Gu et al. 1996) are also plotted in Fig. 9 for comparison. The simulated longitudinal variation of MITC concentration by the laterally averaged 2D model agreed with the field data better than the integral model did. The comparison also indicates that the observed dilution of MITC concentration was quicker than the simulated dilution at a distance of 2,700 m and downstream. The model underestimation of chemical attenuation is attributed to two factors. First, the effects of chemical breakdown and volatilization of MITC were neglected in the simulations. Although MITC, as the main degradation product of Na-MDTC, is more stable than its parent compound in water, the kinetic processes in natural water may become relatively significant compared to the slow dilution resulting from dis-

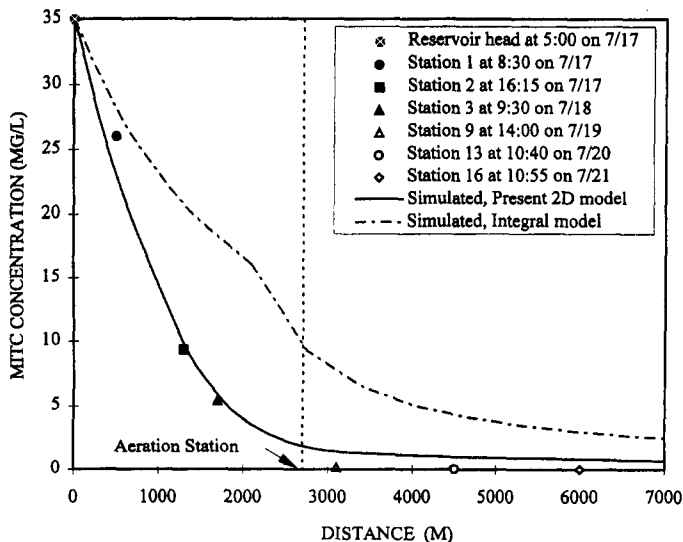


FIG. 9. Observed and Simulated MITC Concentrations at Selected Sampling Stations

TABLE 2. Summary of Observed and Simulated Density Flow Parameters

Flow parameters (1)	Observed (2)	1D model (3)	2D model (4)
Plunge distance (m)	—	—	600
Separation depth (m)	—	9.0	8.5
Separation distance (m)	—	1,900	1,800
Intruding depth (m)	6–9	4.5–8.0	7–8
Intruding thickness (m)	6–7	6.0–9.5	7
Dimensionless concentration at separation point, $C_m/C_0$	0.14	0.4	0.15
Dimensionless concentration at $x = 6$ km (interflow), $C_m/C_0$	0.001	0.09	0.03

persion or mixing in the late stage of flow (interflow). Unfortunately, these kinetic processes have not been well studied and understood (Rosario et al. 1994). Second, a sudden decline of the MITC concentration was observed at a distance of 2,600 m downstream from the reservoir inflow boundary. The sudden drop occurred at the location where the aeration system was installed after the chemical spill to reduce chemical concentrations. These simulation results suggested that the artificial aeration system contributed to the sudden reduction of the MITC concentration to the nondetectable levels in a short time after the spill.

The MITC concentration at a separation point near Sampling Station 3 ( $C_m = 5.25 \text{ mg/L}$ , i.e., dilution factor  $C_0/C_m = 6.67$ ) simulated by the model agreed well with field measurement ( $C_m = 4.9 \text{ mg/L}$ , i.e.,  $C_0/C_m = 7.14$ ), indicating that about 85% dilution was achieved before the contaminated density flow found its equilibrium layer in the Shasta Reservoir. The underprediction of dilution at the separation point by the integral method ( $C_m = 16.8 \text{ mg/L}$  and  $C_0/C_m = 2.08$ ) may result from the underestimation of turbulence and the use of an empirical entrainment coefficient in the underflow analysis.

A summary of observed and simulated contaminant density flow parameters is given in Table 2. The predicted 7–8-m-deep intrusion of interflow was consistent with the observed intrusion depth of 6–9 m. The simulated intruding thickness of 7 m agreed well with the measured ones of 6–7 m. There is relatively good agreement between field measurements and the 2D model results. The 2D model captured the occurrence of different flow regimes and correctly predicted detailed flow behavior and mixing processes, whereas the 1D integral model was capable of predicting only gross behavior. Particularly, the 1D integral model underestimated the dilution of chemical concentration in the underflow and interflow regions.

## CONCLUSIONS

An unsteady, laterally averaged reservoir hydrodynamics and transport model was applied to describe flow behavior and simulate mixing and transport processes of a chemical spill in the Shasta Reservoir, Calif. The occurrence and features of three distinct flow regimes of the contaminated density currents (plunging flow, underflow, and interflow) were successfully captured through 2D numerical simulations of velocity fields and concentration distributions. It was demonstrated that negative buoyancy and ambient stratification played a dominant role during the processes of plunging, separation, and intrusion. The simulation results were compared with field water temperature data and MITC concentration measurements conducted during the spill. The simulated spatial and temporal variations in MITC concentrations and water temperatures correctly predicted the measured features. With limited geometry and flow data, the 2D simulations, particularly for contaminant concentration dilution, agreed with observations better than the 1D integral model predictions did.

Field measurements and 2D simulations showed that about 85% of the MITC concentration dilution was accomplished at the point where the spilled chemical plume separated from the reservoir bed after it plunged into the reservoir from the river. The comparison of simulated and observed MITC concentrations indicated that the aeration system, an artificial mixing device, also contributed to the reduction of MITC concentration downstream to a nondetectable level in a short time after the spill. It was found that after the spill peak passed, higher velocity at the centerline of interflow brought more fresh water to the contaminant plume and led to more dilution in the center than in the side layers of the plume.

## APPENDIX I. REFERENCES

- Akiyama, J., and Stefan, H. G. (1984). "Plunging flow into a reservoir: theory." *J. Hydr. Engrg.*, ASCE, 110(4), 484–499.
- Alavian, V., Jirka, G. H., Denton, R. A., Johnson, M. C., and Stefan, H. G. (1992). "Density currents entering lakes and reservoirs." *J. Hydr. Engrg.*, ASCE, 118(11), 1464–1489.
- Alavian, V., and Ostrowski, P., Jr. (1992). "Use of density current to modify thermal structure of TVA Reservoirs." *J. Hydr. Engrg.*, ASCE, 118(5), 688–706.
- Barnese, L. E., Neichter, P. L., and Bohanon, J. A. (1993). "Evaluation of water quality in Caesar Creek Lake, Ohio using the CE-QUAL-W2 water quality model." U.S. Army Corps of Engrs., Louisville, Ky.
- Buchak, E. M., and Edinger, J. E. (1984). "Generalized longitudinal-vertical hydrodynamics and transport: development, programming and application." U.S. Army Corps of Engrs. Waterways Experiment Station, Vicksburg, Miss.
- Chaudhry, M. H. (1993). *Open-channel flow*. Prentice-Hall, Inc., Englewood Cliffs, N.J.
- Chow, V. T. (1959). *Open-channel hydraulics*. McGraw-Hill, New York, N.Y.
- Chung, S. W. (1996). "Simulation and analysis of density flows and contaminant transport in a stratified reservoir," MS thesis, Dept. of Civ. and Constr. Engrg., Iowa State Univ., Ames, Iowa.
- Cole, T. M. (1982). "Application of the LARM two-dimensional computer model to canyon reservoir," MS thesis, Southwest Texas State Univ., San Marcos, Tex.
- Cole, T. M., and Buchak, E. M. (1994). "CE-QUAL-W2: a two-dimensional, laterally averaged, hydrodynamic and water quality model, version 2.0 user's manual." U.S. Army Corps of Engrs., Waterways Experiment Station, Vicksburg, Miss.
- Draper, W. M., and Wakeham, D. E. (1993). "Rate constants for metam-sodium cleavage and photodecomposition in water." *J. Agric. Food Chem.*, 41, 1129–1133.
- Edinger, J. E., Buchak, E. M., and Merritt, D. H. (1983). "Longitudinal-vertical hydrodynamics and transport with chemical equilibria for Lake Powell and Lake Mead." *Salinity in watercourses and Reservoirs*, R. H. French, ed., Butterworth Publishers, Stoneham, Mass., 213–222.
- Environmental and Hydraulics Laboratory (1986). "CE-QUAL-W2: A numerical two-dimensional, laterally averaged model of hydrodynamics and water quality: user's manual." *Instruction Rep. E-86-5*, U.S. Army Corps of Engrs., Waterways Experiment Station, Vicksburg, Miss.
- Fang, X., and Stefan, H. G. (1991). "Integral jet model for flow from an open channel into a shallow lake or reservoir." *Project Rep. 315*, St. Anthony Falls Hydraulic Lab., Univ. of Minnesota, Minneapolis, Minn.
- Farrell, G. J., and Stefan, H. G. (1989). "Mathematical modeling of plunging reservoir flows." *J. Hydr. Res.*, 26(5), 525–536.
- Fischer, H. B., List, E. J., Koh, R. C. Y., Imberger, J., and Brooks, N. H. (1979). *Mixing in inland and coastal waters*. Academic Press, Inc., New York, N.Y.
- Ford, D. E., and Johnson, M. C. (1983). "An assessment of reservoir density currents and inflow processes." *Tech. Rep. E-83-7*, U.S. Army Corps of Engrs., Waterways Experiment Station, Vicksburg, Miss.
- Gu, R., McCutcheon, S. C., and Wang, P. (1996). "Modeling reservoir density underflow and interflow from a chemical spill." *Water Resour. Res.*, 32(3), 695–705.
- Hebbert, B., Imberger, J., Loh, I., and Patterson, J. (1979). "Collie river underflow into the Wellington reservoir." *J. Hydr. Div.*, ASCE, 105(5), 533–545.
- Imberger, J. (1982). "Reservoir dynamics modeling." *Prediction in water*

- quality*, O'Loughlin, E. M. and Cullen, P., ed., Australian Acad. of Sci., Canberra, Australia, 223–248.
- Imberger, J., and Hamblin, P. F. (1982). "Dynamics of lakes, reservoirs and cooling ponds." *Ann. Rev. Fluid Mech.*, 14, 153–187.
- Johnson, T. R., Ellis, C. R., and Stefan, H. G. (1989). "Negatively buoyant flow in a diverging channel. IV: Entrainment and dilution." *J. Hydr. Engrg.*, ASCE, 115(4), 437–456.
- Johnson, T. R., Ellis, C. R., Farrell, G. J., and Stefan, H. G. (1987). "Negatively buoyant flow in a diverging channel. Part 2: 3-D flow field descriptions." *J. Hydr. Engrg.*, 113(6), 731–742.
- Lide, D. R. (1992). *CRC Handbook of Chemistry and Physics*. CRC Press, Inc., Ann Arbor, Mich.
- Martin, J. L. (1987). "Application of a two-dimensional model of hydrodynamics and water quality (CE-QUAL-W2) to DeGray Lake, Arkansas." *Technical Rep. E-87-1*, U.S. Army Engrs. Waterways Experiment Station, Vicksburg, Miss.
- McKee, C. P., Thackston, E. L., Speece, R. E., Wilson, D. J., and Cardozo, R. J. (1992). "Modeling of water quality in Cheatham Lake." *Technical Rep. 42*, Envir. and Water Resour. Engrg., Vanderbilt Univ., Nashville, Tenn.
- Mossman, D. J., Schnoor, J. L., and Stumm, W. (1988). "Predicting the effects of a pesticide release to the Rhine River." *J. Water Pollution Control Federation*, 60(10), 1806–1812.
- Oriob, G. T. (1983). "Mathematical modeling of water quality: stream, lakes, and reservoirs." *International series on applied system analysis*, Vol. 12, John Wiley & Sons, New York, N.Y.
- Rosario, A., Remoy, J., Soliman, V., Dhaliwal, J., Dhoot, J., and Perera, K. (1994). "Monitoring for selected degradation products following a spill of VAPAM into the Sacramento River." *J. Envir. Qual.*, 23, 279–286.
- Schnoor, J. L., Mossman, D. J., Borzilov, V. A., Novitsky, M. A., Voszhennikov, O. I., and Gerasimenko, A. K. (1992). "Mathematical model for chemical spills and distributed source runoff to large rivers." *Fate of pesticides and chemicals in the environment*, J. L. Schnoor, ed., John Wiley & Sons, New York, N.Y., 347–370.
- Van Gils, J. A. (1988). "Modeling of accidental spills as a tool for river management." *Proc., 1st Int. Conf. on Chemical Spills and Emergency Mgmt. at Sea*, Kluwer Academic Publishers Group, Norwell, Mass., 405–414.
- Worthing, C. R. (ed.). (1987). *The pesticide manual*. 8th Ed., The British Crop Protection Council, U.K.
- Zepp, R. G., and Cline, D. M. (1977). "Rates of direct photolysis in aquatic environment." *Envir. Sci. and Technol.*, 11(4), 359–366.

## APPENDIX II. NOTATION

The following symbols are used in this paper:

- $A_x$  = longitudinal momentum dispersion coefficient;  
 $B$  = waterbody width;  
 $B_n$  = water surface width;  
 $C$  = laterally averaged constituent concentration;  
 $C_m$  = maximum or centerline concentration;  
 $C_{SS}$  = concentration of suspended solids;  
 $C_{TDS}$  = concentration of total dissolved solids;  
 $C_0$  = peak concentration at inflow boundary;  
 $D_x$  = longitudinal temperature and constituent dispersion coefficient;  
 $D_z$  = vertical temperature and constituent dispersion coefficient;  
 $g$  = gravitational acceleration;  
 $h$  = total depth of reservoir;  
 $n$  = free water surface location;  
 $P$  = pressure;  
 $q$  = lateral boundary flow;  
 $q_c$  = lateral mass flow rate of constituent per unit volume;  
 $S_c$  = kinetic source/sink term for constituent concentration;  
 $T_w$  = water temperature;  
 $t$  = time;  
 $U$  = longitudinal velocity;  
 $W$  = vertical velocity;  
 $x$  = longitudinal Cartesian coordinate;  
 $z$  = vertical Cartesian coordinate;  
 $\rho$  = density; and  
 $\tau_x$  = shear stress.